Cement and Concrete Research 42 (2012) 105–110

Contents lists available at SciVerse ScienceDirect

Cement and Concrete Research

journal homepage: http://ees.elsevier.com/CEMCON/default.asp

High pressure study of low compressibility tetracalcium aluminum carbonate hydrates $3CaO \cdot Al_2O_3 \cdot CaCO_3 \cdot 11H_2O$

Juhyuk Moon [a], Jae Eun Oh [b], Magdalena Balonis [c], Fredrik P. Glasser [c], Simon M. Clark [d,e], Paulo J.M. Monteiro [a,*]

[a] Department of Civil and Environmental Engineering, University of California, Berkeley, CA 94720, USA
[b] School of Urban and Environmental Engineering, Ulsan National Institute of Science and Technology, Ulsan Metropolitan City, 689-798, South Korea
[c] Department of Chemistry, Meston Building, University of Aberdeen, Aberdeen, AB24 3UE Scotland, UK
[d] Advanced Light Source, Lawrence Berkeley National Laboratory, Berkeley, CA 20015, USA
[e] Department of Earth and Planetary Sciences, University of California, Berkeley, CA 94720, USA

ARTICLE INFO

Article history:
Received 6 April 2011
Accepted 17 August 2011

Keywords:
Crystal structure (B)
X-ray diffraction (B)
Mechanical properties (C)
Monosulfates (D)

ABSTRACT

Synchrotron X-ray diffraction data was collected from a sample of monocarboaluminate $3CaO \cdot Al_2O_3 \cdot CaCO_3 \cdot 11H_2O$ from ambient pressure to 4.3 GPa. The refined crystal structure at ambient pressure is triclinic with parameters a = 5.77(2) Å, b = 8.47(5) Å, c = 9.93(4) Å, α = 64.6(2)°, β = 82.8(3)°, γ = 81.4(4)°, and space group of *P*1 or $P\bar{1}$. It showed some degree of perfectly reversible pressure-induced dehydration with a non-hygroscopic pressure-transmitting medium. However the dehydration effect does not critically affect a bulk modulus due to its strong framework. The isothermal bulk modulus of monocarboaluminate was found to be 53(5) GPa and 54(4) GPa with 3rd order and 2nd order Birch-Murnaghan Equation of state, respectively. That value is higher than for any other reported AFm or AFt phase. The pressure–volume behavior of the monocarboaluminate was compared with that of previous studied hemicarboaluminate.

1. Introduction

The AFm (Al_2O_3–Fe_2O_3-mono) phases in Portland cements and blended Portland cement are chemically and mineralogically complex. AFm phases have a layered structure derived from that of portlandite, $Ca(OH)_2$, whereby one third of Ca^{2+} ions are replaced by a trivalent ion of Al^{3+} or Fe^{3+}. The principal layer has the chemical formula $[Ca_2(Al,Fe)(OH)_6]^+$. Its interlayer structure with contents $[XnH_2O]$- incorporates variable amounts of water as well as charge-balancing X anions, such as hydroxyl, chloride, carbonate, sulfate, and silicate. The type of the X anion and the amount of interlayer water determine the layer thickness c′, which can be varied stepwise by dehydration at different temperature and humidity conditions [1–3].

Carbonate sources in Portland cement arise from numerous sources: from kiln dust, calcite, impurity in gypsum, or simply by reaction with the atmosphere to form carbonate-containing AFm phases, *e.g.* monocarboaluminate ($C_4A\bar{C}H_{11}$, triclinic, P1 or $P\bar{1}$) [4,5] and hemicarboaluminate ($C_4A\bar{C}_{0.5}H_{12}$, trigonal, R 3 c or R3c) [6]. These varied sources of potential carbonate are sufficient to stabilize hemicarboaluminate or monocarboaluminate, or both in fresh and nominally uncarbonated cement. Monocarboaluminate is stable in contact with calcite, $CaCO_3$, but hemicarboaluminate is stable only over a limited range of CO_2 activities. Thus the hemicarboaluminate is not often observed in real concrete systems due to the difficulty of excluding CO_2 [7]. Damidot et al. [8] showed that with rising carbonate activity, hydroxyl-AFm was replaced first by hemicarboaluminate and then by monocarboaluminate. Thus small amounts of carbonate can influence the nature and stability of the AFm phase, although hemicarboaluminate and monocarboaluminate contain only 3.8 and 7.7 wt.% CO_2, respectively. Of particular interest to the constitution of modern cement paste is the formation of ettringite as a consequence of carbonate additions to cement: sulfate displaced from AFm in the course of forming hemicarboaluminate and monocarboaluminate contributes to the formation of ettringite [6,7].

The variable interlayer contents and layer thickness of monocarboaluminate at varying temperature were studied by Fischer and Kuzel [9] and are shown in Table 1. In the temperature range 95–130 °C (i) the interlayer molecular water of the compound is released in two steps and (ii) the crystallinity degrades. As the crystallinity deteriorates, the corresponding diffraction peak of lamellar distance becomes diffuse. A lower hydrate with the approximate composition $C_4A\bar{C}H_8$ and a layer thickness of $c' = 7.2$ Å is formed at 100 °C, and at 130 °C a phase of composition $C_4A\bar{C}H_6$ with the interlamellar peak of 6.3 Å appears, which corresponds to the phase whereby all the interlayer water molecules have been lost. After that the X-ray reflections become progressively more diffuse until the phase is amorphitized at 250 °C.

As summarized in Table 1, the basic structures of carbon-containing AFm phases have been determined and refined for several

* Corresponding author.
E-mail address: monteiro@berkeley.edu (P.J.M. Monteiro).

0008-8846/$ – see front matter © 2011 Elsevier Ltd. All rights reserved.
doi:10.1016/j.cemconres.2011.08.004

Table 1
Crystallographic data of monocarboaluminate.

	System	Space group	Drying conditions	Layer thickness (Å)	a (Å)	b (Å)	c (Å)	α (°)	β (°)	γ (°)	V (Å^3)	Z	
$C_4A\bar{C}H_{11}$[a]	Triclinic	$P1/P\bar{1}$	25 °C	7.56	5.781(1)	5.744(1)	7.855(1)	92.61(2)	101.96(2)	120.09(2)	217.3	1/2	[9]
$C_4A\bar{C}H_8$[a]			95 °C	7.2	–	–	–	–	–	–	–	1/2	
$C_4A\bar{C}H_6$[a]			130 °C	6.6	–	–	–	–	–	–	–	1/2	
D-$C_4A\bar{C}H_{11}$[a]	Triclinic	$P\bar{1}$	25 °C	–	5.7422(4)	5.7444(4)	15.091(3)	92.29(1)	87.45(1)	119.55(1)	432.52(1)	1	[5]
O-$C_4A\bar{C}H_{11}$[a]		$P1$	25 °C	7.55	5.775(1)	8.469(1)	9.923(3)	64.77(2)	82.75(2)	81.43(2)	433.0(2)	1	[4]
$C_4A\bar{C}H_{11}$[b]	Triclinic	$P1/P\bar{1}$	25 °C	–	5.768	5.742	7.862	92.68	101.89	120.01	217.17[c]	1/2	[14]
$C_4F\bar{C}H_{12.18}$[b]	Rhombohedral	$R\,\bar{3}c$	20 °C	7.98	5.9196(1)	–	47.880(1)	–	–	–	1453.01(4)	6	[13]
$C_4A\bar{C}H_{11}$[b]	Triclinic	$P\,1/\,P\bar{1}$	25 °C	7.59	5.77(2)	8.47(5)	9.93(4)	64.6(2)	82.8(3)	81.4(4)	433(3)	1	t.s

Note: t.s this study.
[a] Single crystal X-ray diffraction.
[b] Power X-ray diffraction.
[c] Calculated from given lattice parameters.

subtypes using powder or single-crystal X-ray diffraction [4,5,9–14]. The resulting charge imbalance gives the main layers a net positive charge, with the result that the interlayer spacing is much greater than in portlandite due to the need to intercalate charge-balancing anions. The layer thicknesses indicate that the CO_3^{2-} ions are oriented sub-parallel to the principal layers in monocarboaluminate but perpendicular to them in hemicarboaluminate. In all these CO_3^{2-} containing phases, some octahedral cavities contain a CO_3^{2-} ion while others contain varying combinations of H_2O molecules and OH^- ions. Francois et al. [4] reported detailed atomic structures of the ordered type of monocarboaluminate using single-crystal X-ray diffraction: among the five water molecules contained in the interlayer, two can be considered as only slightly bonded, and strong hydrogen bonds between O atoms in carbonate groups and water molecules provide cohesion of the interlayer (Fig. 1). In addition, the planar CO_3^{2-} groups are themselves tilted by 21.8(9) degree with respect to the planes formed by the principal calcium aluminate layers. The disordered monocarboaluminate structure, which has a pseudohexagonal symmetry, was also solved through single-crystal X-ray diffraction, [5]. The main difference between these two modifications is the presence or absence of a center of symmetry and the order of stacking layers. When the structure is centrosymmetric, $P\bar{1}$, the compound is disordered and pseudohexagonal. When the structure is noncentrosymmetric P1, the structure is ordered but with a less pronounced pseudohexagonal nature. In the structure of Fe-containing monocarboaluminate, the carbonate location is different, bonding to the main layer in Al-containing monocarboaluminate while weakly bonded and in the interlayer in Fe-containing monocarboaluminate [13].

The stability of monocarboaluminate and hemicarboaluminate has an impact on the bulk chemistry of cements in terms of the formation of ettringite. Several studies reported that this results in a higher volume of hydrated phases, which can contribute to the improvement in mechanical properties of cement pastes [6,7,15]. However, very little has been published on the mechanical properties of the AFm-phases due to their mineralogical complexity and lack of adequate measuring techniques. Previous research has described the structural behavior of hemicarboaluminate and strätlingite under hydrostatic pressure [16] where both AFm phases experienced pressure-induced dehydration, resulting in an abrupt volume contraction around 1.5 GPa. Reported herein is a study of the behavior of the monocarboaluminate under pressure using diamond anvil cell and high-pressure synchrotron X-ray diffraction. In addition, the pressure–volume behavior and bulk modulus of the monocarboaluminate are computed and compared with those of hemicarboaluminate.

2. Experimental procedure

The monocarboaluminate was synthesized from calcium carbonate and tricalcium aluminate. Both materials were mixed in a 1:1 molar ratio and agitated in double distilled, CO_2 free water with

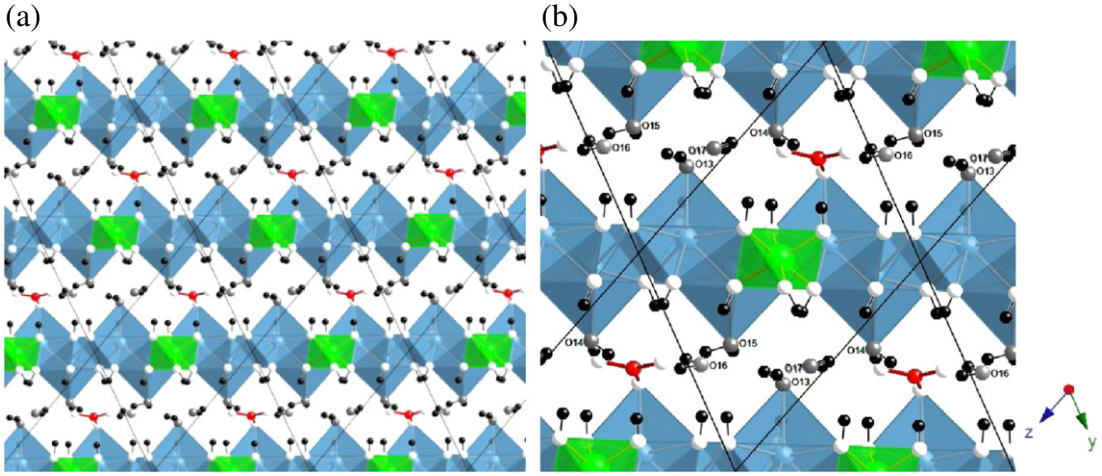

Fig. 1. Projection along [100] of the monocarboaluminate [4]; (a) general view, and (b) detail of interlayer region. Blue and green polyhedra are, respectively, sevenfold Ca polyhedra and sixfold Al polyhedra. White, gray, red, blue, green, and black spheres represent, respectively, O atoms in principal layers, O atoms in interlayers, C, Ca, Al, and H atoms.

water/solid ratio of 10 at 25 °C. After 14 days, the solid was filtered under nitrogen and subsequently dried in a "desiccator" over saturated calcium chloride [6].

Ambient condition phase identification and the high-pressure powder X-ray diffraction experiment were carried out at beamline 12.2.2 of the Advanced Light Source [17], using a synchrotron monochromatic X-ray beam. The National Bureau of Standards LaB_6 powder diffraction standard was used to calibrate the working distance between the sample and detector. For ambient X-ray diffraction, a 400.7570 mm sample to detector distance, X-ray wavelength of 0.6199 Å, and exposure time of 300 s were chosen. Both ambient and high-pressure diffraction patterns were collected using a MAR345 image plate (Fig. 2).

High pressures were generated using a two-screw diamond anvil cell. The sample was finely ground and mixed in a glove box (to avoid carbonation) with a pressure medium of silicone oil (a mixture composed of polysiloxane chains with methyl and phenyl groups) and a few chips of ruby [6]. The mixed sample was placed into a sample chamber hole of a steel-gasketed diamond anvil cell. The sample chamber size was 180 μm diameter with 75 μm thickness. The sample was equilibrated in the diamond anvil cell for about 20 min at each pressure. For this high-pressure experiment, a 357.1010 mm sample to detector distance and X-ray wavelength of 0.4965 Å were used. Exposure times of 600 s were sufficient to give adequate signals for high-pressure powder diffraction patterns. The tested pressure range was 0.1–4.3 GPa, and diffraction patterns were collected with incremental rising and falling pressure. The pressure was measured at off-line using the ruby fluorescence technique [18]. The two-dimensional data were integrated with the Fit2D program, which produced the relative scale intensity [19]. The MAR345 image plate detector was used in order to perfectly define the background, to observe very weak diffraction peaks, and to improve the accuracy of the integrated intensities by achieving a better powder average (Fig. 2).

3. Results

The ambient X-ray diffraction pattern of monocarboaluminate is shown in Fig. 3. The accurate peak positions were obtained using the Fit–Marqardt function in XFit [20], and a unit-cell volume was calibrated using the Celref program [21]. The positions and relative intensities of ambient X-ray reflections of the monocarboaluminate agree with the data of Francois et al. [4]. Thirty-six diffraction peaks were used to refine the unit-cell volume. Ambient crystallographic data of monocarboaluminate is shown in Table 1. The refined crystal structure is triclinic symmetry with parameters $a = 5.77(2)$ Å, $b = 8.47(5)$ Å, $c = 9.93(4)$ Å, $\alpha = 64.6(2)°$, $\beta = 82.8(3)°$, $\gamma = 81.4(4)°$, and $V = 433(3)$ Å^3. Because of the high-resolution synchrotron X-ray diffraction, more diffraction peaks than the one calibrated with $Z = 1/2$ [14] appeared. Thus by using the O–$C_4A\overline{C}H_{11}$ data [4] (*i.e.*, ordered-monocarboaluminate of triclinic crystal system, $P1/\overline{P1}$ space group, and $Z = 1$) as a starting refinement structure, the lattice parameters and volume of ambient monocarboaluminate were successfully refined.

X-ray stacking plots in the 2θ range of 3°–18° and 3.5°–6.0° are shown in Figs. 4 and 5. The calculated lattice parameters of lengths and angles as a function of pressure are shown in Table 2 and Figs. 6 and 7. In the diamond anvil cell, the error ranges of calculated unit-cell volume increased at high pressure (Fig. 8). This might be due to its lower symmetry of monocarboaluminate or to a peak broadening effect in the diamond anvil cell. Thus a weighted linear least-squares fit with errors was applied to the data to assess both pressure and volume errors [22]. The pressure-normalized volume data were fitted by a second and third order Birch–Murnaghan equation of state (B.M. EoS) [23].

In contrast with the other AFm phases, the data did not show any abnormal compressibility or amorphization effect [16], thus the bulk modulus of monocarboaluminate could be calculated over the whole pressure range. However, since the unit-cell volume of the sample experienced some degree of unexpected volume contraction during the unloading process, only loading points were selected to compute the bulk modulus, K_0 and its first derivative, K_0'. The initial volume for B.M. EoS at the point of a convergence was estimated at a value of 433(2) Å^3 [24], which is exactly same as the refined ambient volume. Finally, the second order B.M. EoS and third order B.M. EoS were fitted to the experimental points with $R^2 = 0.991$ and 0.990 fitting convergence, as shown in Fig. 8. In the third order B.M. EoS the bulk modulus of 53(5) GPa with its derivative of 5.02 (non-dimensional constant) were obtained. When the first pressure derivative, K_0', is fixed at 4.0 (*i.e.*, a second order B.M. EoS) it yields a bulk modulus of 54(4) GPa.

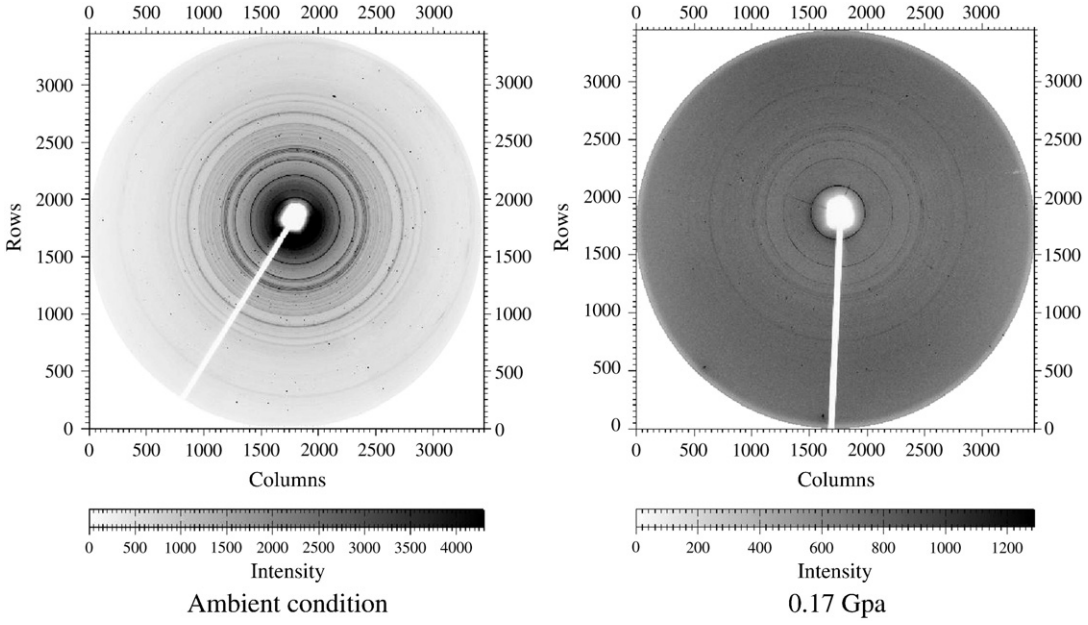

Fig. 2. Raw X-ray powder diffraction patterns collected on monocarboaluminate at ambient condition and 0.17 GPa within DAC, and recorded with MAR345 image plate detector.

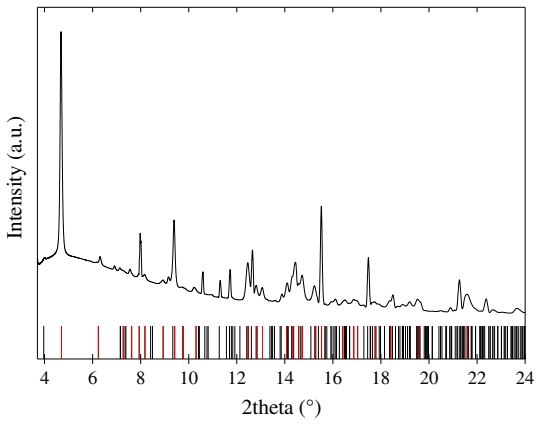

Fig. 3. Ambient X-ray diffraction pattern of monocarboaluminate reported in the 2θ range 3–24° (λ = 0.6199 Å). The vertical lines are Bragg peaks positions from [4]. Red vertical lines were used to refine the unit-cell volume.

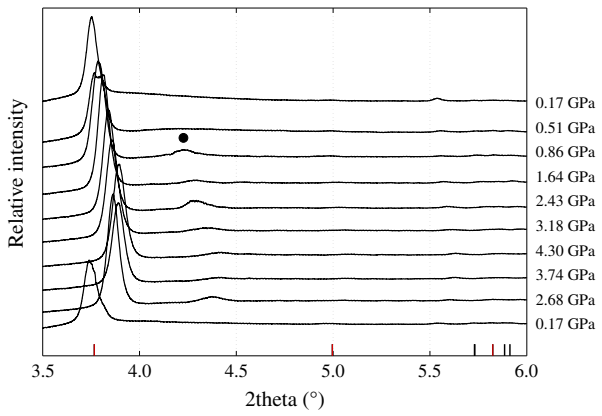

Fig. 5. Interlamellar distance of monocarboaluminate as a function of pressure, reported in the 2θ range 3.5–6.0° (λ = 0.4965 Å). The below three patterns were collected during decompression. The black circle indicates new diffraction peak.

4. Discussion

In previous study, both the hemicarboaluminate and strätlingite experienced pressure-induced dehydration at about 1.0 GPa that much affected their bulk modulus [16]. However monocarboaluminate has no significant dehydration effect. The interlamellar distance of 7.59 Å gradually decreased, however, a single diffraction peak was newly observed at 0.86 GPa (Fig. 5). The exact peak position is 6.7311 Å, which disappeared when it was fully relaxed. Considering the stepwise hydration of monocarboaluminate, this feature also might be due to the pressure-induced dehydration. Since very small amounts of monocarboaluminate dehydrated (*i.e.*, the interlamellar distance remains the same), the newly emerging peak was not included in calculating the bulk modulus. This minute amount of dehydration might be due to movement of water molecules number 16 and 17 from the interlayer (Fig. 1). Based on the previous study on the refinement of atomic structure of the monocarboaluminate, these two waters are not directly connected to the calcium and aluminum oxide polyhedra [4]. On the other hand, the remaining water molecules number 13, 14 and 15 form strong hydrogen bonds with an O atom of a carbonate group, which makes cohesion between the interlayer and principal layer (Fig. 1). Thus these two weakly bonded interlayer waters might be partly moved out from the interlayer of the samples causing an abrupt contraction of its interlamellar distance. Otherwise, considering the *d*-spacing data from the thermal dehydration of monocarboaluminate [9] (Table 1), the 6.6 Å diffraction peak corresponds to that of $C_4A\bar{C}H_6$, which is similar in position to the newly emerging peak at 0.86 GPa. Because this dehydrated monocarboaluminate does not have any water molecules in its interlayer region, only a small portion of the samples might experience full dehydration. Note that the interlamellar distance cannot be directly compared with the experimental points because the peak itself is moving under pressure (*i.e.*, the newly emerging peak should be compared with interlamellar distance of $C_4A\bar{C}H_6$ under 0.86 GPa, not under ambient pressure).

Comparison of the bulk modulus of monocarboaluminate with hemicarboaluminate is summarized in Table 3. According to [16], hemicarboaluminate might experience two complex pressure behaviors; pressure-induced dehydration at about 1.0 GPa and re-orientation of carbonate group. Thus, after the de-hydration of the hemicarboaluminate, it still shows a nonlinear pressure behavior due either to the re-orientation of carbonate groups or to additional dehydration. These effects make the abnormal value of pressure derivative, K_0', 13.6. In addition, the hydrogen bonds in hemicarboaluminate increase in strength as the interlayer space contracts, which yields an almost double bulk modulus relative to that of hemicarboaluminate at ambient. One observation of note is that the pressure–volume curve of monocarboaluminate has a similar slope with that of dehydrated hemicarboaluminate (*i.e.*, after some degree of dehydration of hemicarboaluminate; Fig. 9). In this stage, although the exact atomic position of carbonate group in hemicarboaluminate has not been identified yet, the direction of the group can become parallel to the main layer due to the pressure effect [16]. This re-orientation of

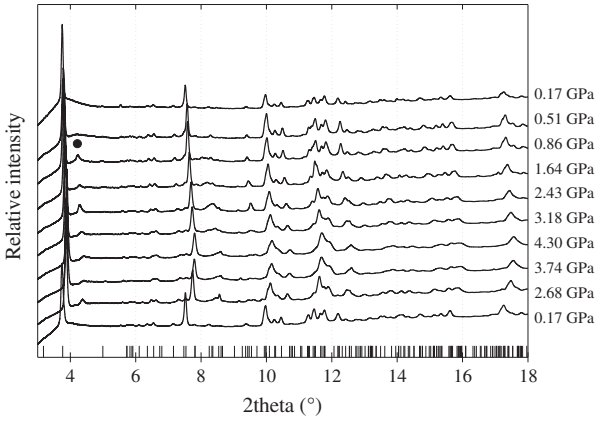

Fig. 4. Integrated powder patterns of monocarboaluminate as a function of pressure, reported in the 2θ range 3–18° (λ = 0.4965 Å). The below three patterns were collected during decompression. The vertical lines are Bragg peaks positions from [4]. The black circle indicates a new diffraction peak.

Table 2
Unit-cell parameters of monocarboaluminate at investigated pressures.

P (GPa)	a (Å)	b (Å)	c (Å)	α (°)	β (°)	γ (°)	V (Å^3)
Ambient	5.77(2)	8.47(5)	9.93(4)	64.6(2)	82.8(3)	81.4(4)	433(3)
0.17(1)	5.76(2)	8.49(3)	9.92(3)	64.6(2)	82.4(3)	81.3(3)	433(3)
0.51(1)	5.73(1)	8.46(3)	9.89(3)	64.8(2)	82.4(3)	81.3(3)	428(2)
0.86(1)	5.72(1)	8.45(3)	9.87(3)	64.8(2)	82.4(3)	81.2(3)	426(2)
1.6(2)	5.71(2)	8.41(3)	9.83(4)	65.0(2)	82.2(3)	81.2(3)	422(3)
2.4(2)	5.69(2)	8.37(4)	9.78(4)	65.1(2)	82.3(3)	81.1(3)	416(3)
3.1(9)	5.66(3)	8.34(5)	9.74(5)	65.2(3)	82.3(4)	81.3(4)	412(4)
4.3(3) [a]	5.64(5)	8.27(9)	9.66(9)	65.4(5)	82.7(8)	80.4(8)	403(7)
3.7(3)[a]	5.64(5)	8.26(8)	9.68(8)	65.3(5)	82.7(8)	80.4(8)	404(7)
2.6(2)[a]	5.64(3)	8.35(6)	9.73(6)	65.2(3)	82.4(5)	80.9(5)	410(5)
0.1(1)[a]	5.77(2)	8.48(4)	9.93(4)	64.7(2)	82.4(3)	81.2(3)	434(3)

Note: Standard deviations in parentheses.
[a] Data points during unloading.

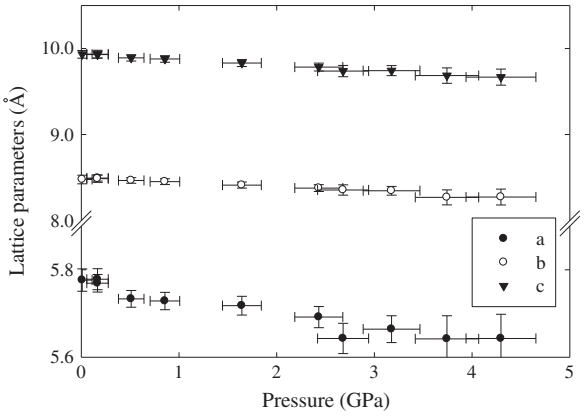

Fig. 6. Variations of lattice parameters of a, b, and c as a function of pressure.

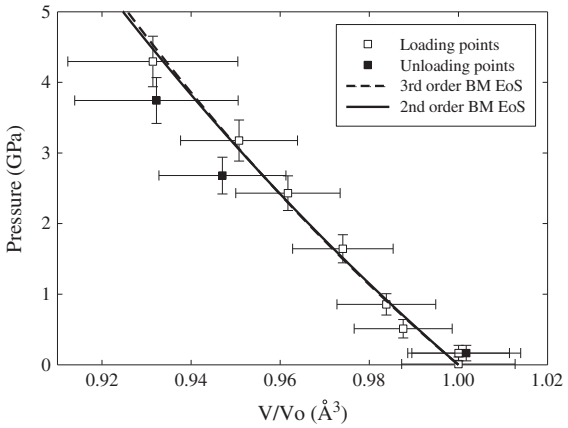

Fig. 8. Pressure-dependent behavior of unit-cell volume normalized to the ambient volume. Open and closed symbols correspond to loading and unloading points. Third order B.M. EoS and second order B.M. EoS fitting give bulk modulus of 53(5) and 54 (4) GPa, respectively.

carbonate group can contribute to the abnormal pressure behavior. Eventually it will make a similar structural framework with monocarboaluminate except for the different positioning of the carbonate group. However, although the similar curve of dehydrated hemicarboaluminate and monocarboaluminate is particularly noteworthy above 1 GPa, the bulk moduli of the dehydration of hemicarboaluminate and monocarboaluminate are still quite different: 32(2) and 54(4) GPa, respectively. From this observation we conclude that the orientation of carbonate groups in the interlayer plays a key role in their bulk moduli.

This difference can be explained by an applied regression method on the hemicarboaluminate. The bulk modulus of second-phase hemicarboaluminate is a result of fitting the experimental points to the 'initial' point of 1.1 GPa, *i.e.*, this yields the bulk modulus at 1.1 GPa with abnormal pressure derivative K_0'. Thus if it contains any interlayer water or perpendicular carbonate groups at 1.1 GPa, the actual bulk modulus at a higher pressure will be definitely greater than 32(2) GPa.

Fig. 9 shows the difference between loading and unloading data points in both samples. Differences might be due to experimental error (*i.e.*, the relaxation time of silicone oil was not sufficient to equilibrate the solution) or additional dehydration induced by pressure during the unloading process. As shown, the dehydration effect is relatively weak for monocarboaluminate because of its intrinsically lower compressibility. In addition, although there can be some time-delayed dehydration effect during the unloading process, the dehydration effect is perfectly reversible. This is completely consistent with the previous research on strätlingite and hemicarboaluminate in a non-hygroscopic pressure medium.

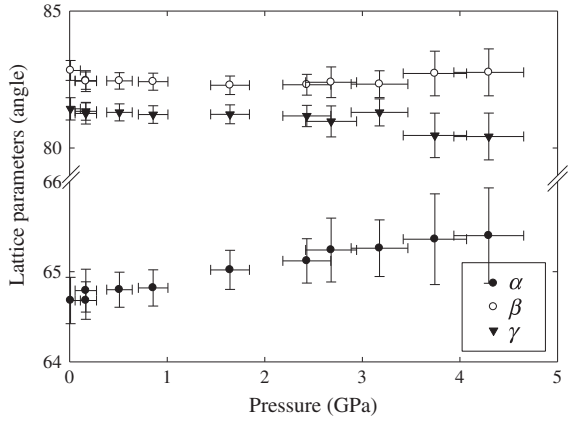

Fig. 7. Variations of lattice parameters of α, β, and γ as a function of pressure.

An exceptionally high bulk modulus was computed for the monocarboaluminate. It is less compressible not only when compared to other AFm phases (strätlingite and hemicarboaluminate) but also to ettringite ($Ca_6Al_2(SO_4)_3(OH)_{12}\cdot 26(H_2O)$, trigonal, a = 11.23 Å, c = 21.44 Å, bulk modulus: 27(7) GPa, [25]), and portlandite ($Ca(OH)_2$, hexagonal, a = 3.5853(7) Å, c = 4.895(3) Å, bulk modulus: 37.8(1) GPa, [26]). In addition, the bulk modulus is still larger than that of dehydrated hemicarboaluminate. Therefore, the bulk modulus of AFm phases is more dependent on its atomistic structural framework than the type of charge-balancing anion species in their interlayer region or the number of interlayer water molecules. This supports the fact that monocarboaluminate is stable not only thermodynamically but mechanically, because of its strong hydrogen bonds with sub-parallel carbonate groups in its interlayer. Although the amount of monocarboaluminate in concrete systems is normally small, these results should stimulate interest in conducting high pressure studies of other main concrete constituents such as calcium monosulfoaluminate hydrates.

5. Conclusions

Monocarboaluminate and hemicarboaluminate occur as hydration products of Portland cement. Small amounts of carbonate can influence the stability and mechanical properties of the AFm phases. In constrast to strätlingite and hemicarboaluminate, monocarboaluminate did not show any significant dehydration or amorphization effect at elevated pressure. In comparing the calculated bulk modulus of monocarboaluminate, 54(4) GPa with that of hemicarboaluminate, 32(2) GPa, not only did the charge-balancing anion species and the number of interlayer water molecules play a key role in determining its mechanical properties, but its atomistic structural framework also contributed. The newly emerging diffraction peak and difference between some loading and unloading points indicate that there is a small degree of pressure-induced dehydration effect under hydrostatic pressure for both hemicarboaluminate and monocarboaluminate. But for monocarboaluminate, it had little effect on its bulk modulus because of its framework that consists of strong hydrogen bonds between interlayer waters and O atoms in carbonate groups.

Acknowledgments

This publication was based on work supported in part by Award No. KUS-l1-004021, made by King Abdullah University of Science and Technology (KAUST). The Advanced Light Source is supported by the Director, Office of Science, Office of Basic Energy Sciences, of

Table 3
Comparison of Bulk modulus and its first derivative of monocarboaluminate with hemicarboaluminate.

	Pressure transmitting medium	Pressure range (GPa)	Initial Volume (Å^3)	K_o'	K_o (GPa)	fixed K_o'	K_o (GPa)
Monocarboaluminate	Silicon oil	0.1–4.3	433(2)	5.02	53(5)	4	54(4)
Hemicarboaluminate [16]	Silicon oil	0.1–1.1	1418.04(1)	n.d	n.d	4	15(2)
		1.1–5.4	1361.25	4.19	32(7)	4	32(2)
	Methanol:Ethanol = 4:1	0.1–1.8	1418.94(4)	13.6	9(2)	4	14(1)
		1.8–4.2	1351.57	4.0	30(3)	4	31(1)

Note: n.d: not determined.

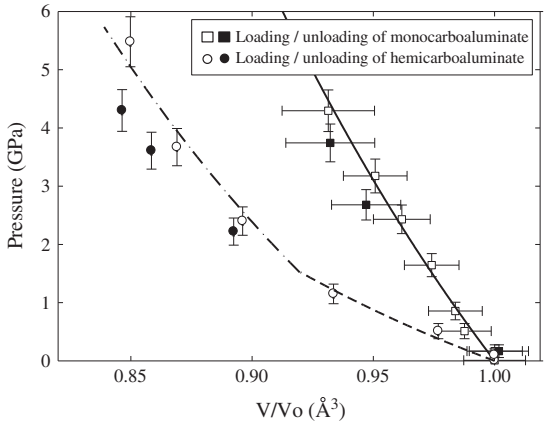

Fig. 9. Pressure–volume behaviors of monocarboaluminate and hemicarboaluminate with silicone oil. Open and closed symbols correspond to loading and unloading points. The lines show second order B.M. EoS fitting.

the U.S. Department of Energy under Contract No. DE-AC02-05CH11231.

References

[1] H.F.W. Taylor, Crystal structures of some double hydroxide minerals, Mineral. Mag. 39 (1973) 377–389.
[2] R. Allman, Chimica 24 (1970) 99.
[3] H.F.W. Taylor, Cement Chemistry, 2nd edition Thomas Telford, London, 1997.
[4] M. François, G. Renaudin, O. Evrard, A cementitious compound with composition $3CaO.Al_2O_3.CaCO_3.11H_2O$, Acta Crystallogr., Sect. C 54 (1998) 1214–1217.
[5] G. Renaudin, M. Francois, O. Evrard, Order and disorder in the lamellar hydrated tetracalcium monocarboaluminate compound, Cem. Concr. Res. 29 (1999) 63–69.
[6] T. Matschei, B. Lothenbach, F.P. Glasser, The AFm phase in Portland cement, Cem. Concr. Res. 37 (2007) 118–130.
[7] T. Matschei, B. Lothenbach, F.P. Glasser, The role of calcium carbonate in cement hydration, Cem. Concr. Res. 37 (2007) 551–558.
[8] D. Damidot, S. Stronach, A. Kindness, M. Atkins, F.P. Glasser, Thermodynamic investigation of the $CaO–Al_2O_3–CaCO_3–H_2O$ closed system at 25 °C and the influence of Na2O, Cem. Concr. Res. 24 (1994) 563–572.
[9] R. Fischer, H.J. Kuzel, Reinvestigation of the system $C_4A·nH_2O–C_4A·CO_2·nH_2O$, Cem. Concr. Res. 12 (1982) 517–526.
[10] R. Allmann, Die Doppelschichtstruktur der plaettchenfoermigen Calcium–Aluminium–Hydroxysalze am Beispiel des 3CaO·Al2O3·CaSO4·12H2O, Neues Jb Mineralog. Monatsh. (1968) 140–144.
[11] F.G. Buttler, L.S.D. Glasser, H.F.W. Taylor, Studies on $4CaO·Al_2O_3·13H_2O$ and the related natural mineral hydrocaluminate, J. Am. Ceram. Soc. 42 (1959) 121–126.
[12] R. Allmann, Refinement of the hybrid layer structure [Ca2Al(OH)6] + ·[1/2SO4·3H2O]−, Neues Jb Mineralog. Monatsh. (1977) 136–144.
[13] B.Z. Dilnesa, B. Lothenbach, G. Le Saout, G. Renaudin, A. Mesbah, Y. Filinchuk, A. Wichser, E. Wieland, Iron in carbonate containing AFm phases, Cem. Concr. Res. 41 (2011) 311–323.
[14] M. Balonis, F.P. Glasser, The density of cement phases, Cem. Concr. Res. 39 (2009) 733–739.
[15] B. Lothenbach, G. Le Saout, E. Gallucci, K. Scrivener, Influence of limestone on the hydration of Portland cements, Cem. Concr. Res. 38 (2008) 848–860.
[16] J. Moon, J. Oh, M. Balonis, F.P. Glasser, S.M. Clark, P.J.M. Monteiro, Pressure induced reactions amongst calcium aluminate hydrate phases, Cem. Concr. Res. 41 (2011) 571–578.
[17] M. Kunz, A.A. MacDowell, W.A. Caldwell, D. Cambie, R.S. Celestre, E.E. Domning, R.M. Duarte, A.E. Gleason, J.M. Glossinger, N. Kelez, D.W. Plate, T. Yu, J.M. Zaug, H.A. Padmore, R. Jeanloz, A.P. Alivisatos, S.M. Clark, A beamline for high-pressure studies at the Advanced Light Source with a superconducting bending magnet as the source, J. Synchrotron Radiat. 12 (2005) 650–658.
[18] H.K. Mao, J. Xu, P.M. Bell, Calibration of the ruby pressure gauge to 800 kbar under quasi-hydrostatic conditions, J. Geophys. Res. 91 (1986) 4673–4676.
[19] A.P. Hammersley, S.O. Svensson, M. Hanfland, A.N. Fitch, D. Hcousermann, Two-dimensional detector software: from real detector to idealised image or two-theta scan, High Pressure Res. 14 (1996) 235–248.
[20] R.W. Cheary, A.A. Coelho, Programs XFIT and FOURYA, deposited in CCP14 Powder Diffraction Library, Engineering and Physical Sciences Research Council, Daresbury Laboratory, Warrington, England, http://wwwccp14acuk/tutorial/xfit-95/xfithtm1996.
[21] J. Laugier, B. Bochu, CELREF. Version 3. Cell parameter refinement program from powder diffraction diagram, Laboratoire des Matériaux et du Génie Physique, Ecole Nationale Supérieure de Physique de Grenoble (INPG), France, 2002.
[22] B.C. Reed, Linear least-squares fits wiht errors in both coordinates, Am. J. Phys. 57 (1989) 642–646.
[23] F. Birch, Finite strain isotherm and velocities for single-crystal and polycrystalline NaCl at high pressures and 300 K, J. Geophys. Res. 83 (1978) 1257–1268.
[24] R. Jeanloz, Finite-strain equation of state for high-pressure phases, Geophys. Res. Lett. 8 (1981) 1219–1222.
[25] S.M. Clark, B. Colas, M. Kunz, S. Speziale, P.J.M. Monteiro, Effect of pressure on the crystal structure of ettringite, Cem. Concr. Res. 38 (2008) 19–26.
[26] H.E. Petch, The hydrogen positions in portlandite, $Ca(OH)_2$, as indicated by the electron distribution, Acta Crystallogr. 14 (1961) 950–957.